

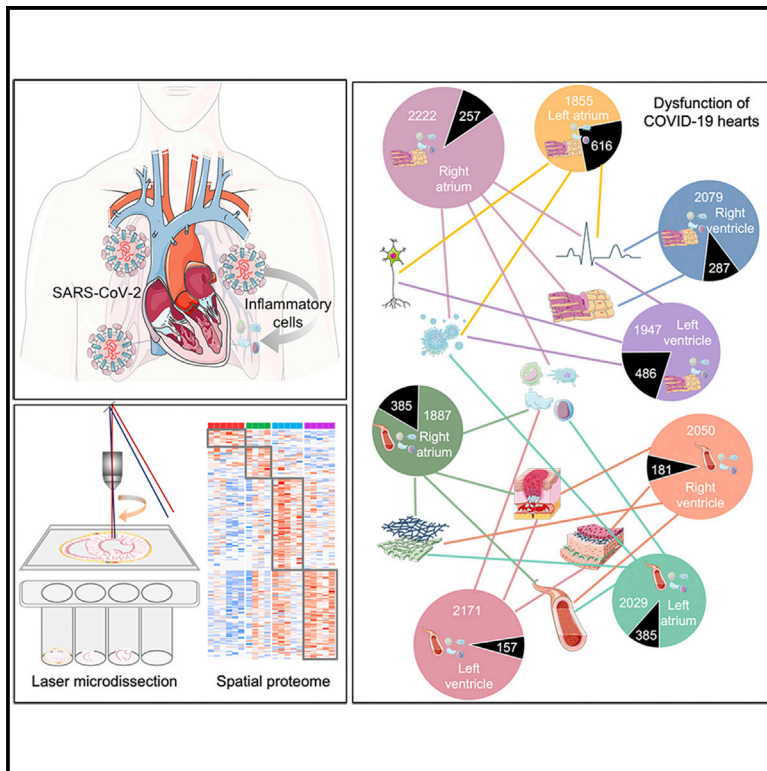


Since January 2020 Elsevier has created a COVID-19 resource centre with free information in English and Mandarin on the novel coronavirus COVID-19. The COVID-19 resource centre is hosted on Elsevier Connect, the company's public news and information website.

Elsevier hereby grants permission to make all its COVID-19-related research that is available on the COVID-19 resource centre - including this research content - immediately available in PubMed Central and other publicly funded repositories, such as the WHO COVID database with rights for unrestricted research re-use and analyses in any form or by any means with acknowledgement of the original source. These permissions are granted for free by Elsevier for as long as the COVID-19 resource centre remains active.

Spatial region-resolved proteome map reveals mechanism of COVID-19-associated heart injury

Graphical abstract



Authors

Ling Leng, Jie Ma, Pei-Pei Zhang, ..., Zhi-Yong Liang, Xiu-Wu Bian, Shu-Yang Zhang

Correspondence

lengling@pumch.cn (L.L.), liangzy@pumch.cn (Z.-Y.L.), bianxiuwu@263.net (X.-W.B.), shuyangzhang103@nrdrs.org (S.-Y.Z.)

In brief

Leng et al. establish a region-resolved proteome map of the inflammatory myocardia and microvessels of COVID-19 hearts. The myocardia and microvessels of the left atrium are the most affected by inflammation storm. These results could provide guidance in improvement of clinical treatments for cardiovascular diseases associated with COVID-19.

Highlights

- Spatial proteome maps of COVID-19 myocardia and microvessels are established
- SARS-CoV-2-driven inflammation leads to region-resolved dysfunction of the heart
- Mechanisms of dysregulated contraction, conduction, and circulation are elaborated
- Myocardia and microvessels of the left atrium are affected by inflammation the most



Resource

Spatial region-resolved proteome map reveals mechanism of COVID-19-associated heart injury

Ling Leng,^{1,11,*} Jie Ma,^{2,11} Pei-Pei Zhang,^{3,4,5,11} Si-Chi Xu,^{6,11} Xiao Li,^{2,11} Ye Jin,^{6,11} Jun Cai,⁷ Rui Tang,⁴ Lei Zhao,⁷ Zhi-Cheng He,⁴ Man-Sheng Li,² Hui Zhang,⁸ Liang-Rui Zhou,⁸ Zhi-Hong Wu,¹ Tian-Ran Li,⁴ Yun-Ping Zhu,^{2,9} Yu-Jie Wang,¹ Hai-Bo Wu,³ Yi-Fang Ping,⁴ Xiao-Hong Yao,⁴ Chu-Hong Zhu,⁵ Hai-Tao Guo,⁴ Le-Yong Tan,⁴ Zhi-Yong Liang,^{8,*} Xiu-Wu Bian,^{3,4,*} and Shu-Yang Zhang^{6,10,12,*}

¹Stem Cell and Regenerative Medicine Lab, Department of Medical Science Research Center, State Key Laboratory of Complex Severe and Rare Diseases, Translational Medicine Center, Peking Union Medical College Hospital, Peking Union Medical College and Chinese Academy of Medical Sciences, Beijing 100730, China

²State Key Laboratory of Proteomics, Beijing Proteome Research Center, National Center for Protein Sciences (Beijing), Beijing Institute of Lifeomics, Beijing 102206, China

³Department of Pathology, The First Hospital Affiliated to University of Science and Technology of China (USTC), Intelligent Pathology Institute, Division of Life Sciences and Medicine, USTC, Hefei, Anhui 230036, China

⁴Institute of Pathology and Southwest Cancer Center, Southwest Hospital, Third Military Medical University (Army Medical University), Key Laboratory of Tumor Immunopathology, Ministry of Education of China, Chongqing 400038, China

⁵Department of Pathology, Ruijin Hospital, Shanghai Jiao Tong University School of Medicine, Shanghai 200025, China

⁶Department of Cardiology, Peking Union Medical College Hospital, Peking Union Medical College and Chinese Academy of Medical Sciences, Beijing 100730, China

⁷Department of Pathology, Shanghai Jiao Tong University School of Medicine, Shanghai 200025, China

⁸Department of Pathology, Peking Union Medical College Hospital, Peking Union Medical College and Chinese Academy of Medical Sciences, Beijing 100730, China

⁹Basic Medical School, Anhui Medical University, Anhui 230032, China

¹⁰Tsinghua-Peking Center for Life Sciences, Tsinghua University, Beijing 100084, China

¹¹These authors contributed equally

¹²Lead contact

*Correspondence: lengling@pumch.cn (L.L.), liangzy@pumch.cn (Z.-Y.L.), bianxiuwu@263.net (X.-W.B.), shuyangzhang103@nrdrs.org (S.-Y.Z.)
<https://doi.org/10.1016/j.celrep.2022.110955>

SUMMARY

Direct myocardial and vascular injuries due to severe acute respiratory syndrome coronavirus 2 (SARS-CoV-2) infection-driven inflammation is the leading cause of acute cardiac injury associated with coronavirus disease 2019 (COVID-19). However, in-depth knowledge of the injury characteristics of the heart affected by inflammation is lacking. In this study, using a quantitative spatial proteomics strategy that combines comparative anatomy, laser-capture microdissection, and histological examination, we establish a region-resolved proteome map of the myocardia and microvessels with obvious inflammatory cells from hearts of patients with COVID-19. A series of molecular dysfunctions of myocardia and microvessels is observed in different cardiac regions. The myocardia and microvessels of the left atrial are the most susceptible to virus infection and inflammatory storm, suggesting more attention should be paid to the lesion and treatment of these two parts. These results can guide in improving clinical treatments for cardiovascular diseases associated with COVID-19.

INTRODUCTION

Among the various organ dysfunctions associated with coronavirus disease 2019 (COVID-19), heart complications are one of the most significant and life-threatening (Chung et al., 2021; Driggin et al., 2020). About 12%–41% of patients with COVID-19 had cardiac injury (Akhmerov and Marbán, 2020; Friedrich and Cooper, 2021; Sandoval et al., 2020). Cardiovascular injury is the most common extrapulmonary organ complication among critically ill patients, and its presentation ranges from mild symptoms of palpitation or chest tightness to viral myocarditis, heart failure,

arrhythmia, cardiogenic shock, and sudden death (Guo et al., 2020; Gupta et al., 2020; Madjid et al., 2020; Ning et al., 2022). Severe acute respiratory syndrome coronavirus 2 (SARS-CoV-2) promotes the abnormal release of pro-inflammatory cytokines and chemokines by activated endothelial cells, monocytes, and lymphocytes. Such virally driven cytokine release may lead to vascular inflammation, plaque instability, myocardial inflammation, direct myocardial suppression, and the formation of a hypercoagulable state (Bonow et al., 2020). Myocarditis caused by SARS-CoV-2 infection has also been proven by induced pluripotent stem cell-derived cardiomyocytes (iPSC-CMs) (Sharma



et al., 2020). SARS-CoV-2 infection can upregulate several inflammation-related genes, including pro-inflammatory cytokine tumor necrosis factor alpha (TNF- α). The pretreatment of iPSC-CMs with TNF- α obviously increased the expressions of angiotensin-converting enzyme 2 (ACE2) and transmembrane protease serine 2 (TMPRSS2) and enhanced the entry of GFP-expressing SARS-CoV-2 pseudovirus into iPSC-CMs, and the neutralization of TNF- α ameliorated the TNF- α -enhanced viral entry, which demonstrated the significant role of the inflammatory reaction during cardiac injury (Lee et al., 2021). However, the specific mechanism underlying myocardial or cardiovascular damage associated with SARS-CoV-2-driven second injury by the infiltrated inflammatory cells remains unknown.

Since the outbreak of COVID-19, proteomics has been widely used to investigate the molecular characteristics and prognosis of injured organs in patients with COVID-19 (Bojkova et al., 2020; Leng et al., 2020, 2021; Nie et al., 2021; Shu et al., 2020; Stukalov et al., 2021). In this study, through a combination of pathology, laser-capture microdissection, and mass spectrometry, proteins of myocardia and microvessels from the four regions of the heart, including left atrial (LA) myocardium (LA_MC), LA microvessel (LA_MV), left ventricular (LV) myocardium (LV_MC), LV microvessel (LV_MV), right atrial (RA) myocardium (RA_MC), RA microvessel (RA_MV), right ventricular (RV) myocardium (RV_MC), and RV microvessel (RV_MV), were isolated and produced a spatial region-resolved proteome map of the human heart. In particular, the proteins from the eight different regions of inflammatory myocardia and microvessels from the hearts of patients with COVID-19 were used to explore the molecular events of myocardial or microvessel tissues mediated by inflammation in SARS-CoV-2-infected hearts, which could provide useful information for the potential drug target and improve the recovery of patients with COVID-19.

RESULTS

Spatial proteome architecture of the resolved human hearts

The heart tissues of patients with COVID-19 showed scattered individual myocyte necrosis with myocardial and perivascular infiltration of lymphocytes and monocytes. The cardiac muscle fibers were thick and interdigitated, and the myocytes were hypertrophic (Figures S1A–S1C). Thrombi were grossly apparent, especially in the capillaries (Figure S1D). Lymphocytic infiltration was observed around small nerves (Figure S1D). To further study the mechanism of SARS-CoV-2 infection affecting specific anatomical parts of the heart, 28 non-COVID-19 (control) and 17 COVID-19 heart samples, including four precise anatomical regions (LA, LV, RA, and RV), were obtained for protein identification (Figures 1A and 1B; Tables S1 and S2). In total, 4,143 proteins were identified in the four regions (Figures S1E and S1F; Table S3). There were 228, 347, 338, and 219 differently expressed proteins in the LA, LV, RA, and RV regions of COVID-19 samples compared with the normal controls, respectively (Figure S1G).

The proteins associated with the inflammatory response were upregulated in four regions, especially in the RA (Figure 1C). In

addition, proteins associated with the coagulation cascade pathway in the RA, RV, and LA were upregulated, whereas those in the LV were downregulated (Figures 1C and 1D), indicating the different abnormal disorders of the coagulation system. Among downregulated proteins, those associated with the extracellular matrix (ECM) remodeling were downregulated markedly in LV (Figure 1D), indicating that the extracellular skeleton of the LV was severely damaged. Muscle-contraction-associated proteins in the RV were downregulated, indicating serious myocardial damage (Figure 1D). Transcription- and translation-associated proteins in the LA and LV were downregulated, whereas those in the RV were upregulated (Figures 1C and 1D), indicating that gene expression and protein synthesis were affected. These results suggest that the inflammatory response of the COVID-19 hearts is abnormally activated, which presents a serious risk factor for cardiac dysfunction.

Proteome profile of inflammatory myocardia and microvessels in COVID-19 hearts

The laser microdissection technology was used to isolate the inflammatory microvessels and myocardia infiltrated by inflammatory cells of the COVID-19 heart tissues (Figure 2A). Overall, 2,376 proteins in the microvessels and 2,494 proteins in the myocardia were identified (Figures 2B–2D; Tables S4 and S5). By correlating the proteins across the myocardia and microvessels in control groups, the proteomes of eight regions could be grouped into two sections: four regions of the myocardia and four regions of the microvessels (Figure 2E). Cellular component analysis revealed that the myocardia were mainly composed of proteins involved in myelin sheath, focal adhesion, mitochondria, sarcomere, Z disc, actin cytoskeleton, sarcolemma, and neuromuscular junction. However, the most important components of the heart microvessels were proteins involved in the ECM, actin cytoskeleton, basement membrane (BM), and neuron projection (Figure 2F). In addition, they contained a large number of proteins associated with myelin sheath, focal adhesion, mitochondria, etc., in the heart microvessels.

Subsequently, proteins in the different regions of microvessels and myocardia in control groups were divided into four parts according to the proportion of protein abundance (quantile [Q] 1: 25%, Q2: 50%, Q3: 75%, Q4: 100%) to identify the protein with specifically high abundance in different regions (Figures 2G and 2H). For the myocardia, results showed that most of the highly expressed proteins (in Q1 or Q2) in different regions were actins (ACTB and ACTA2), muscle myosins (MYH7, MYL4, and TPM1), troponins (TNNT2), creatine kinase (CKM), myoglobin (MB), and atrial natriuretic peptide (NPPA), which were the skeleton and regulators of the muscle or muscle cells (Figure 2G). Other troponins (TNNC1), desmosome (DSP), titin (TTN), thyroid hormone-binding protein (TTR), and the component of a calcium channel (RYR2) were found to be relatively lowly expressed (in Q3 or Q4) in the four regions of myocardia (Figure 2G). For the microvessels, results indicated that most of the highly expressed proteins (in Q1 or Q2) in different regions were spermatogenesis associated (SPATA20), actins (ACTB and ACTA2), type I collagens (COL1A2 and COL1A1), and vimentin (VIM) (Figure 2H). BM components, including type IV collagens (COL4A1 and COL4A2), proteoglycans (HSPG2 and LUM),

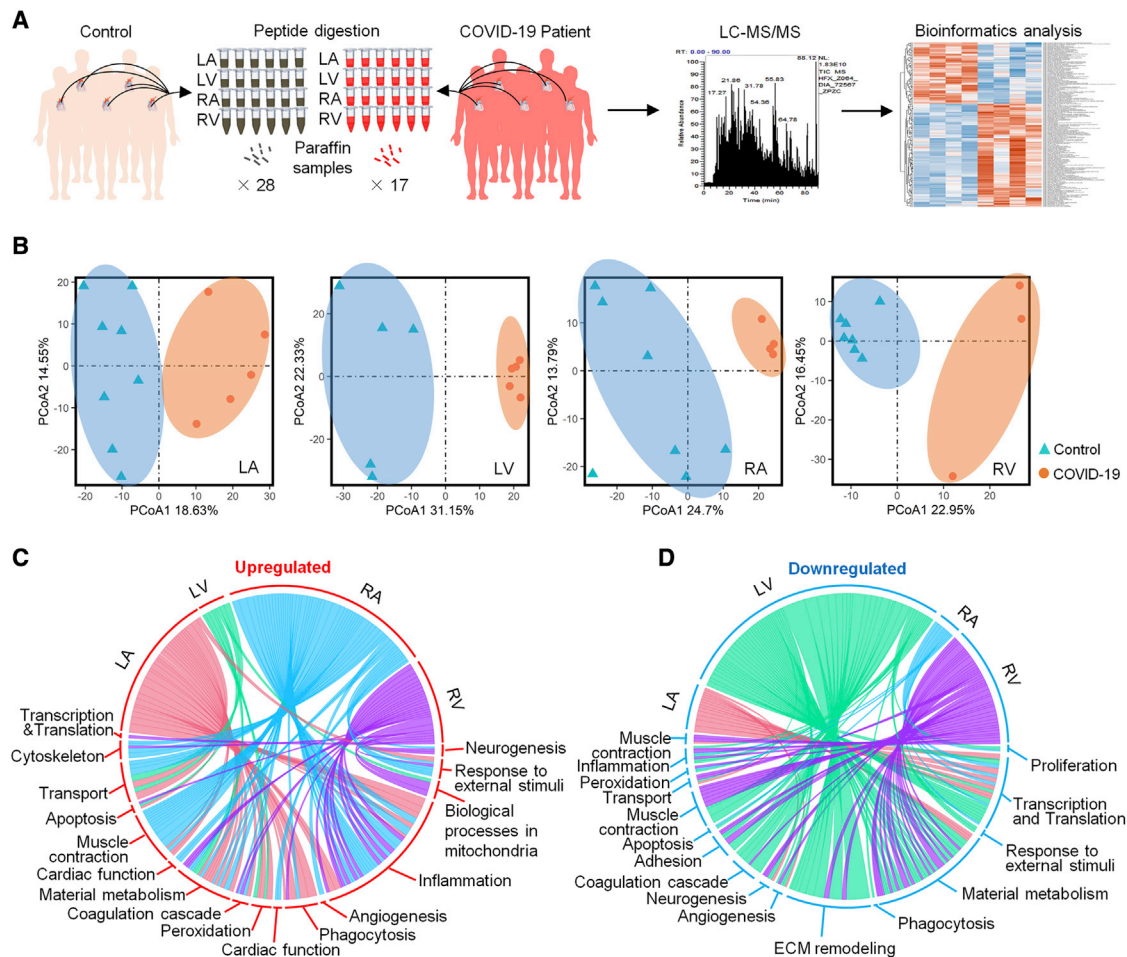


Figure 1. Quantitative proteome profiling of distinct protein signatures in region-resolved heart tissues

(A) Schematic of the experimental workflow of the sample collection, quantitative proteome, and bioinformatics analysis to analyze the four regions of human heart tissues based on anatomy structure in the study: left atrium (LA), left ventricle (LV), right atrium (RA), and right ventricle (RV). Dissected samples from each structure were pooled, digested, and analyzed by liquid chromatography-tandem mass spectrometry (LC-MS/MS).

(B) Principal coordinates analysis (PCoA) analysis of the proteome profile in the four regions of hearts from patients with COVID-19 and normal control subjects. (C and D) Circos diagram shows the biological processes associated with the upregulated (C) and downregulated (D) proteins from four regions of hearts from patients with COVID-19 and normal control subjects. Red, green, blue, and purple lines represent the correlation between multiple biological processes and LA, LV, RA, and RV regions, respectively. The differentially expressed proteins (DEPs) between COVID-19 ($n = 17$) and control ($n = 28$) samples were determined based on the p value of a moderated t test using the R package Limma: $p < 0.01$ and \log_2 COVID-19/control > 1 (upregulated), and $p < 0.01$ and \log_2 COVID-19/control < -1 (downregulated).

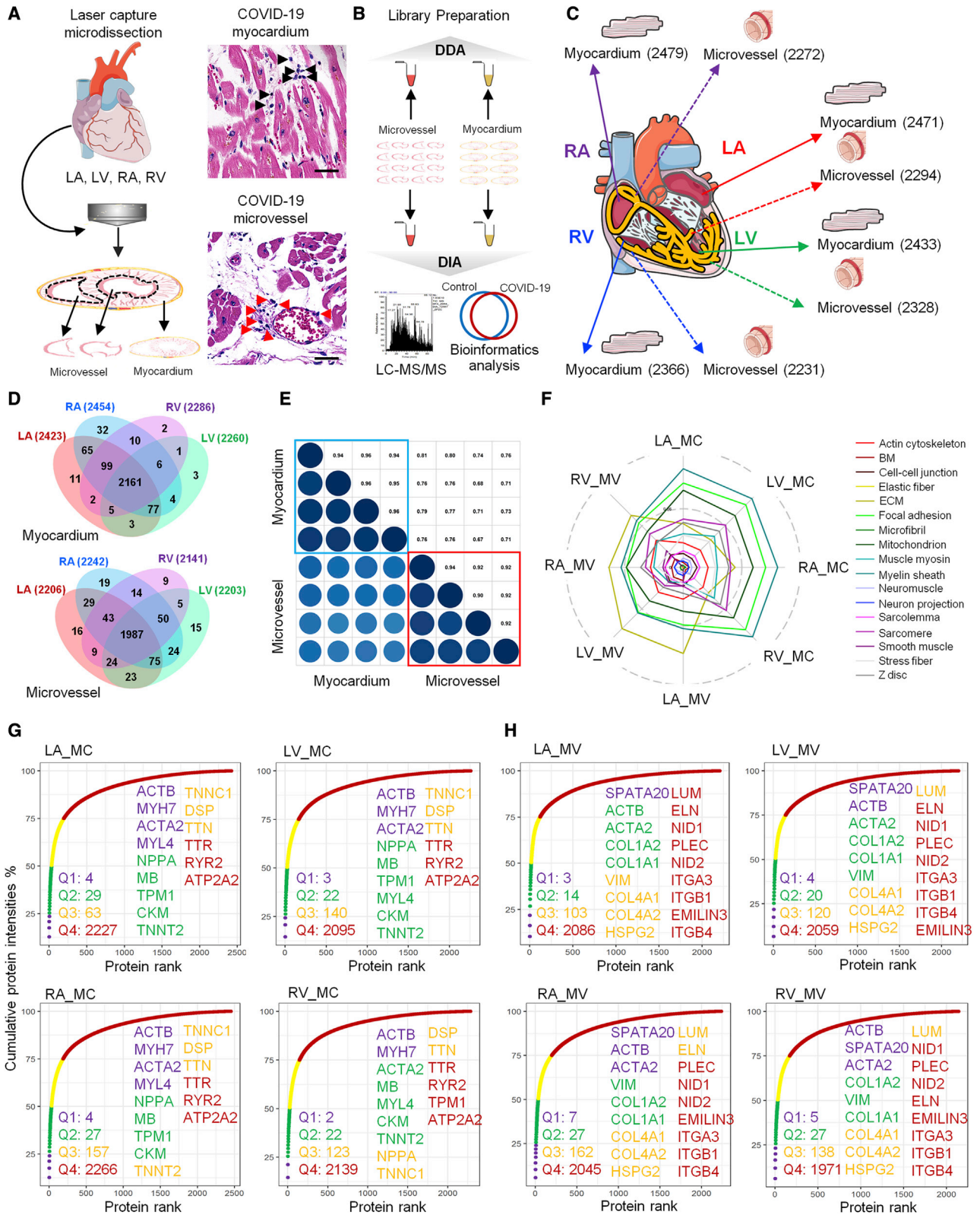
See also [Figure S1](#) and [Tables S1](#) and [S2](#).

elastin and elastin microfibril (ELN and EMILIN3), nidogens (NID1 and NID2), hemidesmosome (PLEC and ITGB4), and integrins (ITGA3 and ITGB1), were relatively lowly expressed (in Q3 or Q4) in the four regions of microvessels ([Figure 2H](#)). A region-resolved proteome profiling system is established, and the specific components of myocardium and microvessel from the four regions are identified, enabling the investigation of the specific functions of human heart in different regions.

Region-resolved functional characteristics of human myocardia

Next, through hierarchical clustering analysis (HCA) and Gene Ontology (GO) analysis, four protein clusters characterizing the

different regions of the myocardia with distinct functions were identified ([Figure 3A](#)). Results indicated that region-specific proteins are linked to the functional difference of myocardia ([Figure 3A](#)). Module 1, representing the proteins highly expressed in the LA of myocardia, was mainly involved in biological functions of protein assembly, response to oxygen levels, microvilli assembly, and transmembrane transport ([Figures 3A, 3B, and S2A](#)). Module 2, representing the proteins highly expressed in the LV of myocardia, was mainly involved in small-molecule metabolism, energy metabolism, protein assembly, cytoskeleton, myocardial contraction, myocardial tissue development, and transmembrane transport ([Figures 3A, 3B, and S2A](#)). The enriched proteins in the RA of myocardia (module 3) were involved



(legend on next page)

in the process of small-molecule metabolism, myocardial contraction, macromolecular metabolism, cell junction, circulation, immune effector, and immune responses, including monocyte-mediated immunity, complement activation, humoral immunity, innate immunity, phagocytosis, and wound healing (Figures 3A, 3B, and S2A). The enriched proteins in the RV of myocardia (module 4) were involved in energy metabolism, cytoskeleton, myocardial contraction, myocardial tissue development, and circulation process (Figures 3A, 3B, and S2A). In addition, a transferrin receptor (TFRC; specifically expressed with high abundance in RA), which is required for erythropoiesis and neurologic development, was selected to verify the proteome results. Results showed that TFRC was specifically expressed in the cytoplasm and cell membrane of the RA_MC (Figure 3C). These results suggest that highly expressed proteins in the myocardia from all four heart regions are involved in small-molecule metabolism, energy metabolism, and cytoskeleton. Highly enriched proteins in the myocardia of both ventricles (RV and LV) are involved in additional biological processes such as myocardial tissue development. Highly enriched proteins in the myocardia of RA are involved in the most specific functions.

Characteristics of inflammatory myocardia in COVID-19 hearts

To further investigate the dysfunction of specific anatomical parts of the COVID-19 myocardia, we identified 2,457 proteins in myocardia of four regions from COVID-19 patients (Figures S3A–S3D; Table S4), with 1,031 proteins differently expressed in the four regions (Figure S3E). Most of the highly expressed proteins in the four regions of the myocardia were downregulated in COVID-19 hearts (Figure 3A), indicating that SARS-CoV-2 infection severely affected the specific function of myocardia in different regions. For example, translocase of inner mitochondrial membrane 50 (TIMM50) was the most significantly downregulated protein among all LA-specific highly expressed proteins in myocardia after SARS-CoV-2 infection, which can lead to cell apoptosis (Reyes et al., 2018). EFHD1, an EF-hand superfamily member of calcium-binding proteins that functions as a mitochondrial Ca^{2+} sensor (Hou et al., 2016), was highly expressed both in LA and LV and significantly downregulated after infection, which enhanced neuronal death (Ulisse et al., 2020). MYBPHL is mostly downregulated in RV-

specific highly expressed proteins, which may increase the risk of human arrhythmias and cardiomyopathy in humans (Barefield et al., 2017). We selected the LV and RA highly expressed proteins PRKCSH and TFRC for verification and found them to be downregulated and upregulated in the CMs of COVID-19, respectively (Figure S3F), which was consistent with the proteome results (Figure 3A).

Next, we investigated the molecular characteristics of myocardial injuries in different regions of the COVID-19 hearts. Results showed that the upregulated proteins between COVID-19 and control groups were involved in inflammatory response, especially in RA myocardia (Figure 4A). For example, acute-phase response-associated proteins (SERPINA3, FN1, and LBP) and innate immune response-associated proteins (KRT16, KRT1, DEFA1, SAMHD1, TUBB4B, and CLU) were highly expressed in the COVID-19 RA myocardia (Figures 4A and 4B). The upregulated proteins involved in the viral process showed the largest number in the RA compared with other regions (Figure 4A), which may be the major cause of the inflammatory response of the RA myocardia. For example, viral life-cycle-associated proteins (CD81, RPL11, RPL35A, RPL24, EIF3F, and RPL8) were highly expressed in the myocardia of RA. The differentially downregulated expressed proteins were mainly involved in energy metabolism and cardiac conduction of all four regions of COVID-19 myocardia (Figure 4A). Abnormal mitochondrial calcium handling, energy failure, and impaired mitophagy may lead to contractile dysfunction of the myocardium. As expected, many proteins associated with muscle contraction, actin cytoskeleton, and myocardial development in LA, LV, RA, and RV were downregulated in the COVID-19 myocardia (Figure S4A), which may lead to heart failure and myocyte death. Cardiac conduction abnormalities have been regarded as sequelae of COVID-19; 10% of the patients with COVID-19 presented with heart palpitations, and 16.7% presented with cardiac arrhythmia (Angeli et al., 2020). Calcium-mediated signaling-associated proteins (PPP3CA, CAMK2D, ATP2B4, NUDT4, and SRL) of LA; membrane potential-associated proteins (MECP2, HEBP2, TSPO, and ADIPOQ) of LA, LV, and RA; and cell communication-associated proteins involved in cardiac conduction (CACNA2D1 and CASQ2) of LV and RV were downregulated in the COVID-19 myocardia (Figure 4B). In addition, myocardial development-associated proteins (GPC1, ANKRD1, PTGFRN, EHD1, and PDLIM5) were

Figure 2. Quantitative proteome profiling of spatially distinct protein signatures in the myocardia (MCs) and microvessels (MVs) of human hearts

- (A) The experimental workflow of the sample collection of MCs and MVs by laser microdissection. Hematoxylin and eosin staining of the COVID-19 MCs and MVs (scale bars, 50 μL). Black and red solid arrows point to the inflammatory cells of MCs and MVs, respectively.
- (B) The experimental workflow of quantitative proteome and bioinformatics analysis to analyze the MCs and MVs from four regions of human heart tissues.
- (C) Total protein numbers of the MCs and MVs from four regions of the control and COVID-19 hearts.
- (D) Venn diagrams show the overlap of the protein numbers identified in the four heart regions (LA, LV, RA, and RV) from the MCs ($n = 27$) and MVs ($n = 20$) of normal controls, respectively.
- (E) Region-dependent analysis of the heart proteomes based on the correlation matrix between the four regions of MCs (LA_MC, LV_MC, RA_MC, and RV_MC) and MVs (LA_MV, LV_MV, RA_MV, and RV_MV), respectively.
- (F) The radar image shows cellular components of the four regions of MCs and MVs based on the protein intensity. Different colors represent the multiple cellular components enriched in the heart tissues.
- (G and H) Cumulative protein abundances for the MCs (G) and MVs (H) of heart regions and the total number of proteins constituting the quantiles (Q1: 25%, Q2: 50%, Q3: 75%, Q4: 100%).

See also Video S1 and Tables S3 and S4.

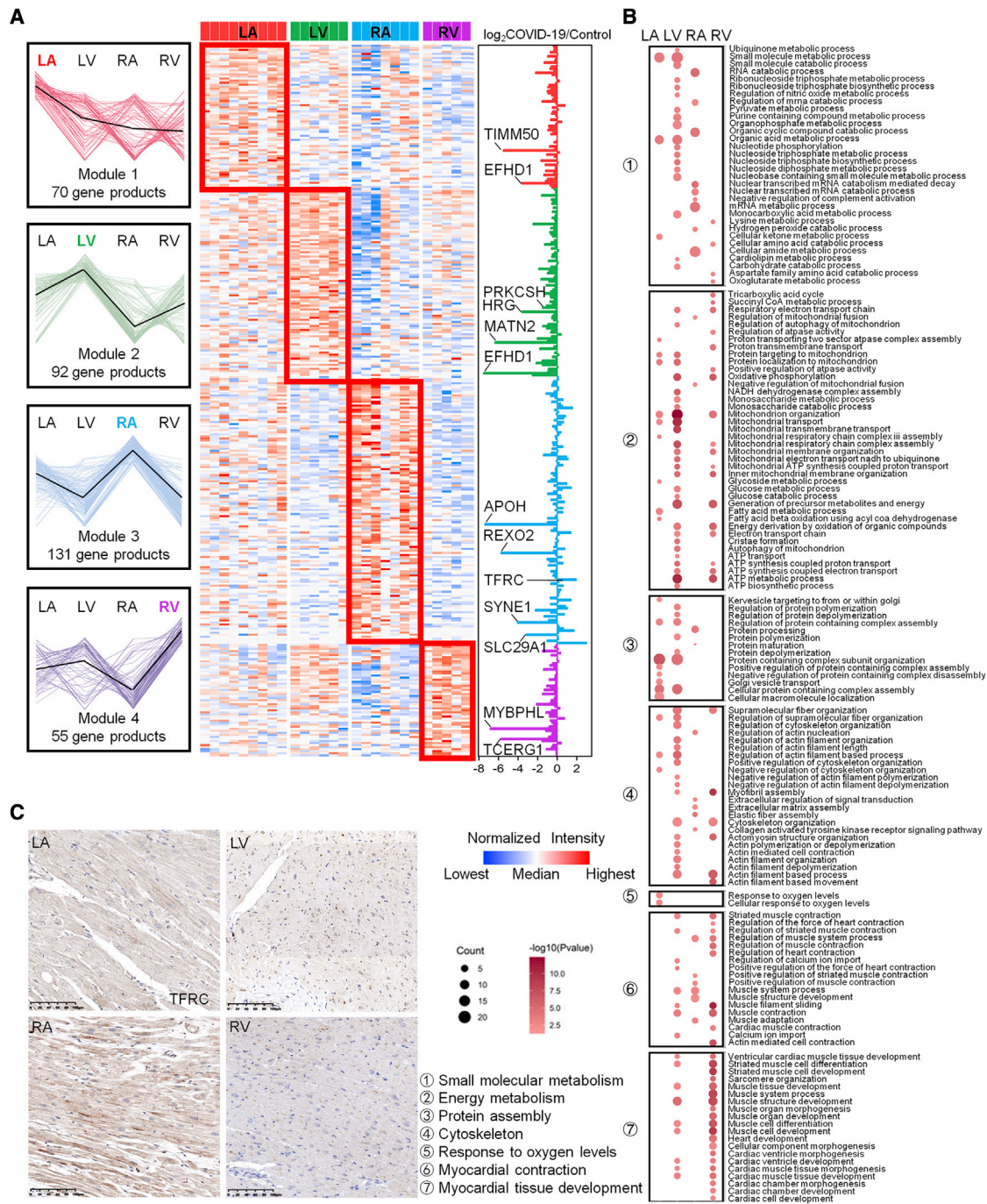


Figure 3. Spatial functional characteristic of region-resolved MCs from human hearts

(A) Four protein modules reveal MC proteomes specificity based on heart structure by co-expression analysis, including LA (n = 9), LV (n = 6), RA (n = 7), and RV (n = 5). The proteins with the one-way ANOVA $p < 0.05$ were regarded as statistically significant in the specific region. Red and blue boxes indicate proteins with increased and decreased abundance, respectively. Left panel: the co-expression patterns of the proteins in the four modules. Histogram on the right represents upregulated or downregulated proteins in the COVID-19 MCs of four regions, compared with those of the normal controls.

(B) Clusters of proteins associated with similar biological processes in the MCs of four heart regions are grouped according to the degree of enrichment. Circles of different sizes represent the number of genes. Gradient red boxes indicate the $-\log_{10} p$ value based on biological processes enrichment.

(C) Immunohistochemistry of the TFRC in the normal MC of LA, LV, RA, and RV (scale bars: 100 μm).

See also [Figures S2](#) and [S3](#).

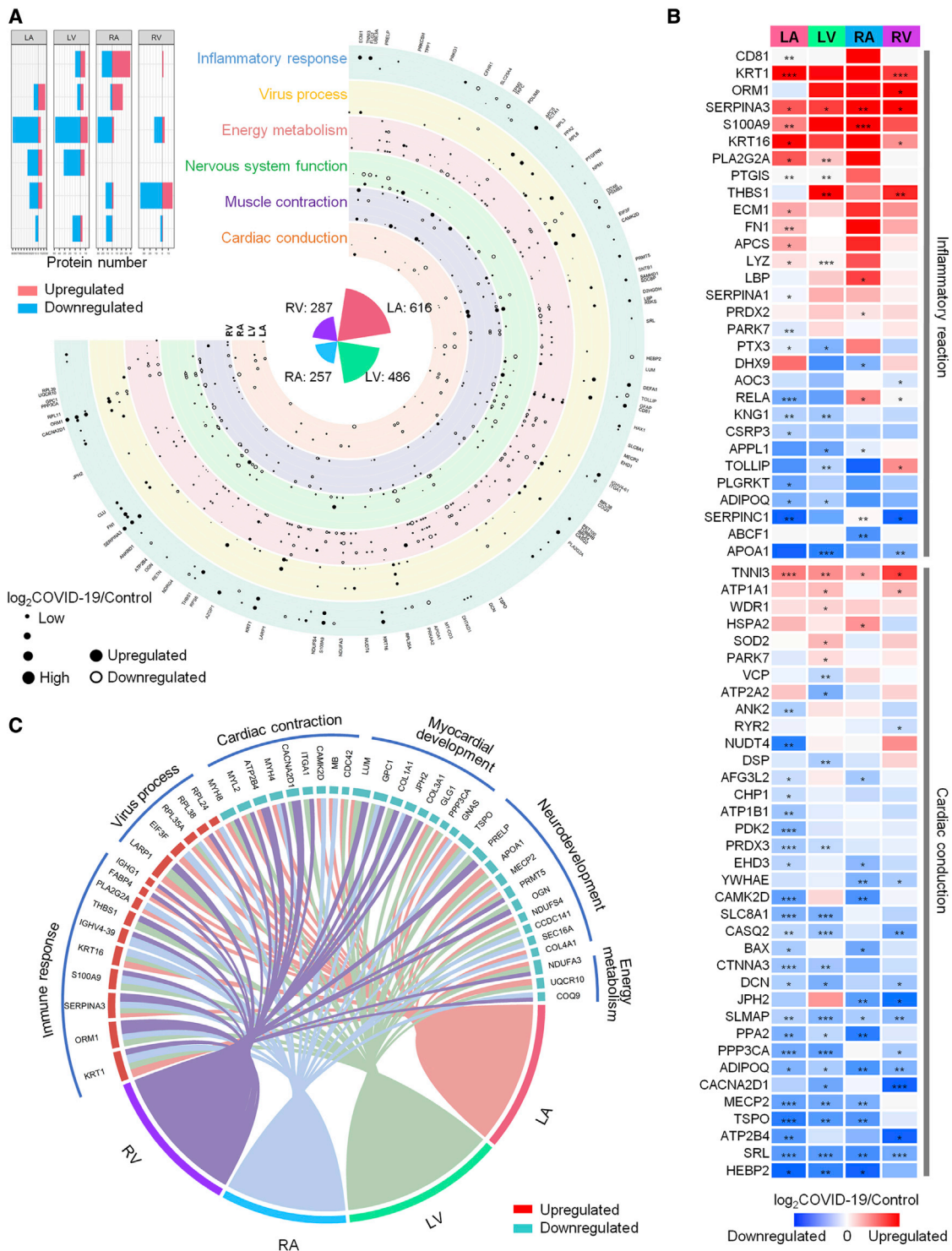


Figure 4. MCs dysfunction in patients with COVID-19 based on the heart spatial proteome profile

(A) Circos diagram shows six function clusters of dysregulated proteins from MCs of four heart regions between patients with COVID-19 and normal controls. Each ring in the function cluster represents the DEPs in a specific heart region. The proteins were considered as significantly dysregulated in four regions with the moderated t test $p < 0.05$. The dysregulated proteins in the six clusters are labeled as circles (solid, upregulated proteins; hollow, downregulated proteins). The size of the circle indicates $|\log_2(\text{COVID-19/control})|$. The function items of the six clusters are presented on the top left corner. The red and blue boxes represent the numbers of upregulated and downregulated proteins, respectively, in the COVID-19 MCs, compared with the normal controls.

(legend continued on next page)

downregulated in the COVID-19 myocardia (Figure S4A), which could be a cause of cardiac conduction dysregulation. These results indicate that myocardial injury in patients with COVID-19 is region specific.

In addition, parts of the molecular characteristics of the four regions of the COVID-19 myocardia were the same. For example, a member of the serpin family A, SERPINA3, which is associated with thrombopoietin signaling via the JAK-STAT pathway and innate immune system, was upregulated in all four regions of the myocardia (Figure 4C). Proteins associated with neurodevelopment, including methyltransferase (PRMT5) in LA, LV, and RV, as well as methyl-CpG binding protein (MECP2) in LA, LV, and RA, were downregulated in the myocardia, which indicated the potential role of methylation in nervous system dysfunction of COVID-19 myocardia (Figure 4C). Together, these results demonstrate that COVID-19 myocardium injuries commonly affect several biological processes and functions of the heart not only with region specificity but also with commonality.

Region-resolved functional characteristics of microvessels in COVID-19 hearts

Next, four protein clusters characterizing different regions of microvessels with distinct functions were identified (Figure 5A). The highly expressed proteins in LA (module 1) were involved in biological functions of material metabolism, antimicrobial response, phagocytosis, oxidative stress, ascorbic acid associated process, and plasma membrane transport (Figures 5A, 5B, and S2B). Module 2, representing the proteins highly expressed in the LV, was mainly involved in the actin filament-based process, vasoconstriction, wound healing, and several immune responses (Figures 5A, 5B, and S2B). Proteins enriched in RA (module 3) were mainly involved in the actin filament-based process, myocyte growth, energy and material metabolism, and microbial response. The highly enriched proteins of RV (module 4) were mainly involved in the processes of muscle contraction, myocyte growth, endothelial cell injury, cardiac conduction, and blood circulation. In addition, the splicing factor 3b subunit (SF3B2) was verified with high expression level in the endothelial cells of microvessels from the LV (Figure 5C). These results suggest that highly expressed proteins in the microvessels from four heart regions are all involved in the function of material metabolism. The highly enriched proteins in RA and RV microvessels are also involved in additional biological processes, such as myocyte growth and energy metabolism. However, most of the biological processes of the highly enriched proteins in the four regions of microvessels are specific, which may be related to the functional differences of microvessels in different regions.

Characteristics of inflammatory microvessels in COVID-19 hearts

We next performed spatial mass spectrometry to identify 2,342 proteins in four regions of microvessels from COVID-19 hearts (Figures S5A–S5D; Table S5), with 745 proteins differently expressed in the microvessels between COVID-19 and control groups (Figure S5E). Most of the specific highly expressed proteins in four regions of microvessels were downregulated after SARS-CoV-2 infection (Figure 5A), indicating dysfunction of microvessels in the COVID-19 hearts. For example, retinoic acid receptor responder 2 (RARRES2), which was the most significantly downregulated protein among all LV-specific highly expressed proteins after SARS-CoV-2 infection, could mediate the formation of microvessels as a vascular endothelial growth factor (Bozaoglu et al., 2010). Sortilin 1 (SORT1), which was associated with the risk of myocardial infarction in humans (Amengual et al., 2018), was downregulated significantly in RV of COVID-19 microvessels. Furthermore, PGD (specifically highly expressed in RV) and SF3B2 (specifically highly expressed in LV) were selected and verified to be downregulated in COVID-19 microvessels (Figure S5F).

Further, we investigate the molecular characteristics of microvessel injuries in the different regions of the heart. Most of the upregulated proteins between COVID-19 and control groups were involved in the inflammatory response, especially in the microvessels of the LA (Figure 6A). Acute inflammatory response-associated proteins (SERPINA3, C7, FN1, PTGIS, PLA2G2A, LYZ, IL17D, and THBS1) and innate immune response-associated proteins (IGHG4 and PSMC6) were upregulated in the COVID-19 microvessels of LA (Figures 6A and 6B). Additionally, the proteins involved in the viral process, such as RPS16, RPL3, SLPI, RPL31, RPL23, RPL24, RPS3A, PTX3, FAU, and RPS23, were the most differentially expressed in LA among the four regions, which may be a major cause of the inflammatory response of microvessels in LA (Figures 6A and 6B). Blood circulation ability-associated proteins were significantly downregulated, especially in the microvessels of the RA, such as TNNI3, CAMK2D, POSTN, MYBPC3, ACTN2, MB, and MYH7 (Figures 6A and S4B). Moreover, the proteins involved in the hypoxia response process of RA were also the most differentially expressed in RA among the four regions (Figure 6A), which may be caused by the deficiency of its blood circulation ability. We also found that the microvessels of LV and RV had the most severe loss of enzyme activity-associated proteins (Figure 6A). The enzyme system is crucial for vascular regeneration. The loss of the enzyme system, such as SERPIND1 of LV and ALDH1A1 of RV (Figure 6A), can lead to poor cardiovascular self-recovery in patients with COVID-19. Additionally, blood pressure and ECM remodeling-associated proteins in the microvessels of four regions

(B) Function analysis of DEPs between the COVID-19 MCs and control samples. Columns on the right of the heatmap represent different functional categories. The left of the heatmap presents the gene names. Red and blue boxes indicate the \log_2 (COVID-19/control) of the up- or downregulated proteins, respectively. Asterisks indicate statistical significance (* $p < 0.05$; ** $p < 0.01$; *** $p < 0.001$), which was determined by the Benjamini-Hochberg (BH)-adjusted p value of a moderated t test between COVID-19 and control samples.

(C) Circos diagram shows upregulated and downregulated proteins that are involved in multiple biological processes of the MCs of four heart regions in patients with COVID-19, compared with those of the normal controls. Red, green, blue, and purple lines represent the correlations between multiple biological processes and LA, LV, RA, and RV regions, respectively. Upregulated expressed proteins: moderated t test $p < 0.05$ and \log_2 COVID-19/control > 1 ; downregulated expressed proteins: moderated t test $p < 0.05$ and \log_2 COVID-19/control < -1 . See also Figures S3, S4, S6, and S7.

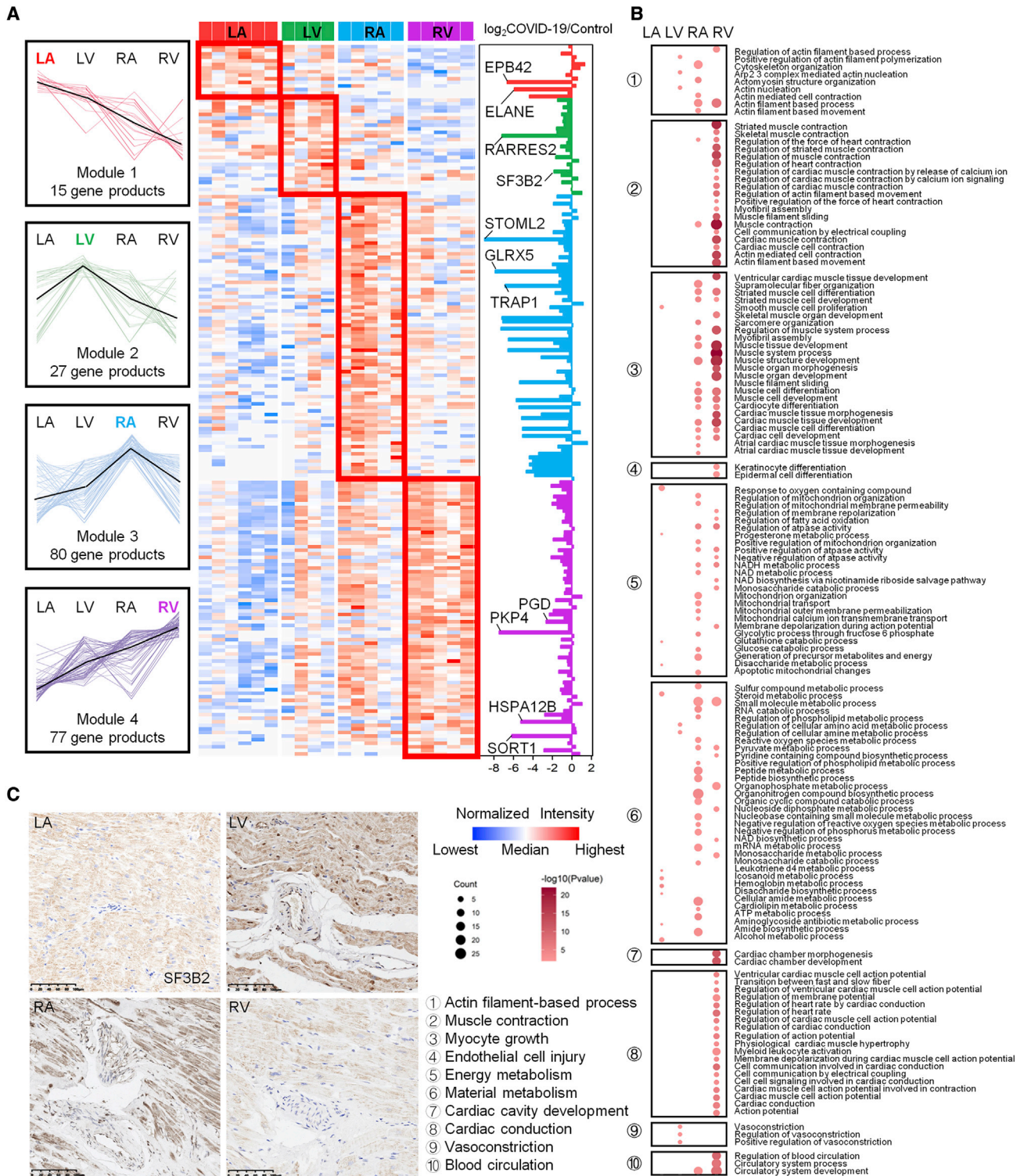


Figure 5. The spatial functional characteristic of region-resolved MVs from human hearts

(A) Four protein modules reveal MV proteomes specificity based on heart structure by co-expression analysis, including LA (n = 6), LV (n = 4), RA (n = 5), and RV (n = 5). The proteins with the one-way ANOVA $p < 0.05$ were regarded as statistically significant in the specific region. Red and blue boxes indicate proteins with increased and decreased abundance, respectively. Left panel: the co-expression patterns of the proteins in the four modules. Histogram on the right represents upregulated or downregulated proteins in the COVID-19 MVs of four heart regions, compared with those of the normal controls.

(legend continued on next page)

are severely dysregulated in COVID-19 heart tissues (Figures 6A and 6B). The coagulation-associated proteins in the microvessels of LV, RA, and RV and the hormone stimulation response-associated proteins of RV were mainly downregulated in COVID-19 microvessels (Figure 6A). Taken together, these results indicate that there are regionally specific injury characteristics of microvessels damage after COVID-19 infection.

In addition, parts of the molecular characteristics of the four regions of the COVID-19 microvessels were similar (Figure 6C). For example, a secretory calcium-dependent phospholipase (PLA2G2A) that plays a role in the regulation of energy metabolism and inflammation was upregulated in the biological processes of immune response from LA, RA, and RV of COVID-19 microvessels. Cathepsin B (CTSB) can be used by SARS-CoV-2 entering TMPRSS2-negative cells (Sungnak et al., 2020). CTSB was upregulated in all four regions of microvessels, indicating the potential role of CTSB in SARS-CoV-2 infection. Together, these results indicate that COVID-19 cardiovascular injuries destroy several biological processes and functions of the heart not only with region specificity but also with commonality.

Effect of SARS-CoV-2 proteins on microvessel function in different heart regions

Next, we found that SARS-CoV-2 can infect microvessels (Figure S5G). To investigate the influence of microvessel function caused by SARS-CoV-2 proteins, we constructed an integrated interactome network between the viral proteins and differentially expressed proteins of the microvessels between COVID-19 and control groups (Figure 7A), following the previous strategy (Leng et al., 2021). The results suggested that viral proteins cause changes of microvessel functions from almost all four regions. Although most of these proteins were identified in all four regions, their expressions levels varied by the effect of interaction with the viral proteins. For example, several proteins related to energy metabolism were interacted with viral proteins; these proteins in the COVID-19 microvessels of RA regions were severely downregulated, such as ATP5F1B, MDH1, and MT-ATP6, whereas the expression of MDH1 in RV was upregulated after SARS-CoV-2 infection. Several proteins with direct interaction of viral proteins are involved in vascular development. For example, the interactions of GNA13 (guanine nucleotide binding protein (G Protein), Alpha 13) with ORF3b, ORF3, and ORF7b function as modulators or transducers in various transmembrane signaling systems. GNA13-deficient mice died at embryonic day 9.5 because of a loss of microvessels (Offermanns et al., 1997). The result showed that GNA13 was significantly downregulated in the microvessels of RA among the four regions, suggesting that the interactions between GNA13 and virus proteins may have great impact on the angiogenesis in RA. The virus proteins had less direct interactions with proteins related to oxygen level, cardiac conduction, inflammatory response, muscle contraction, and ECM remodeling, suggesting that SARS-CoV-2 may

have less impact on these functions. This indicated that these dysfunctions may be caused by virally driven inflammation.

Inflammation-driven ECM characteristics in different regions of the COVID-19 hearts

SARS-CoV-2 infection can lead to heart failure in patients with COVID-19. Heart failure is usually characterized by myocardial fibrosis caused by ECM deposition (Berk et al., 2007). To further investigate how inflammatory myocardium and microvessels lead to ECM changes in four regions of COVID-19 hearts, we used the “Matrisome” database (Shao et al., 2020) to analyze the heart ECM characteristics after SARS-CoV-2 infection. In total, 125 ECMs, including myocardia (53) and microvessels (72), were found to be differently expressed in COVID-19 hearts compared with the normal groups. The expressions of core ECMs, including collagens, glycoproteins, and proteoglycans, were downregulated mostly in the COVID-19 myocardia and were upregulated mostly in the COVID-19 microvessels (Figure S6A). In addition, the expressions of ECM-associated proteins, including ECM regulators, ECM-affiliated proteins, and secreted factors, changed a lot in the microvessels, but a little in the myocardia after SARS-CoV-2 infection. Our results showed that several ECMs associated with coagulation and thrombosis were significantly upregulated in microvessels, especially in LA (THBS1, FN1, FBLN1) and LV (F13A1, THBS1); the anticoagulant reaction-associated ECMs were found to be downregulated mainly in the microvessels (Figure S6B), indicating the dysfunction of the coagulation system in COVID-19 hearts. The BM is an important structure that creates a barrier between cardiac myocytes or endothelial cells and the ECM. The BM components of COVID-19 microvessels, such as LAMB1, LAMC1, and NID2, were downregulated (Figure S6B), which may lead to the shedding of CMs or endothelial cells from the heart tissues. Fibrillar collagen types I and III, as well as the low-abundance collagen types IV, V, and VI, are the main ECMs of the heart (Fan et al., 2012). Results showed that COL1A1, COL1A2, and COL5A1 were upregulated in COVID-19 microvessels that could lead to excessive deposition and affect vasoconstriction (Figure S6B). Furthermore, the enzymes that control the balance between ECM synthesis and degradation to maintain cardiac structural integrity were upregulated in microvessels and myocardia. Most of these enzymes were enzyme inhibitors; for example, SERPINE2 that can inhibit thrombin, urokinase, plasmin, and trypsin and TIMP3 that can inhibit several matrix metalloproteinases were upregulated in RA (Figure S6B). All these indicated that ECMs expressed with high abundance cannot be degraded easily, which would further lead to the excessive deposition of ECM. In contrast, the elastic fiber-associated proteins (FMOD, MFAP5, MFAP2, FBLN5, CILP, and MATN2) and connective tissue homeostasis-associated proteins (PRELP and COL5A3), which are the structural proteins of myocardia, were downregulated mostly in the COVID-19 myocardia (Figure S6B), indicating that myocardial tissues were

(B) Clusters of proteins associated with similar biological processes of MVs in four heart regions are grouped according to the degree of enrichment. Circles of different sizes represent the number of genes. Gradient red boxes indicate the $-\log_{10}$ p value based on biological processes enrichment.

(C) Immunohistochemistry of SF3B2 in the normal MVs of LA, LV, RA, and RV (scale bars: 100 μ m).

See also Figures S2 and S5.

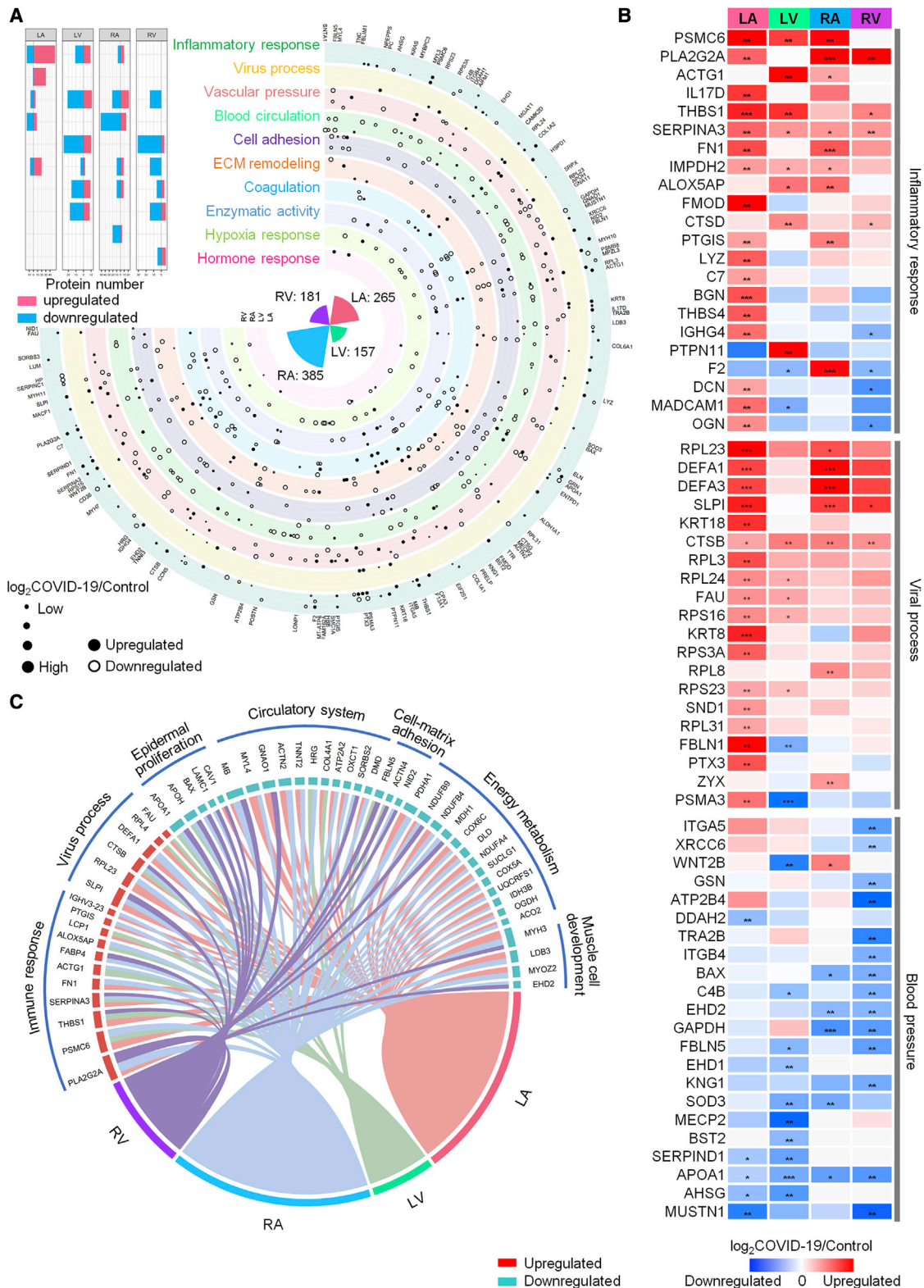


Figure 6. MVs dysfunction of COVID-19 patient based on the heart spatial proteome profile

(A) Circos diagram shows 10 function clusters of dysregulated proteins from MVs of four heart regions between patients with COVID-19 and normal control subjects. Each ring in the function cluster represents the DEPs in a specific heart region. The proteins were considered as significantly dysregulated in four regions

(legend continued on next page)

severely damaged. These results suggest that the dysregulation of ECM may also be an important reason for the inflammation-mediated severe injury of COVID-19 hearts.

Next, we used differentially expressed proteins between COVID-19 sera and hearts for correlation analysis. Results showed that several ECM proteins that were identified in the sera proteome profile and can be used to predict the prognosis of COVID-19 pneumonia were consistent with those differentially expressed between COVID-19 and normal hearts, including in myocardia and microvessels (Figure S7). For example, ECM regulators (HRG, ITIH2, ITIH1, and SERPINC1) and proteoglycan (LUM) that were downregulated in the COVID-19 sera were also decreased in the COVID-19 myocardia and microvessels of four heart regions. The ECM regulator (SERPINA3) that upregulated in the COVID-19 sera was also increased in the COVID-19 myocardia and microvessels. These results indicate that the differentially expressed ECMs identified in the inflammatory myocardium and microvessels of patients with COVID-19 can also be detected in sera of patients with COVID-19; thus, these ECM proteins could be considered as potential markers for heart injury.

DISCUSSION

Usually, pathology is used to analyze the phenotype of heart disease of four chambers. However, there are few studies on the molecular characteristics of specific pathological phenomena in specific heart regions. The molecular composition of microvessels was unclear; therefore, the pathogenesis of cardiovascular-related diseases was difficult to study in detail. The molecular characteristics of the myocardium in different heart regions are unclear, which prevents full understanding of the specific contractility and conduction characteristics of the myocardium.

In this study, our results revealed that although the cell types of the four regions of heart are similar; their molecular composition is specific, which may lead to differences in their functions (Tretter and Redington, 2018). For example, the specific highly expressed proteins of the myocardia from the LV and RV are involved in similar functions, including energy metabolism, myocardial contraction, and myocardial tissue development (Figure 3B). However, LV myocardia were enriched more in small-molecule metabolism, protein assembly, skeleton, and transmembrane transport-associated proteins. In addition, the specific highly expressed proteins in the four regions of microvessels showed several different enriched functions (Figure 5B). RA collects blood from superior and inferior vena of the body, which mainly contains carbon dioxide and waste. Many hypoxia response- and blood cir-

ulation-associated proteins were downregulated, while inflammatory response, blood pressure, and coagulation-associated proteins were upregulated in the microvessels of the RA from COVID-19 hearts (Figure 7B). The blood pressure-associated proteins in RV, which receive blood from RA, were downregulated significantly, suggesting a failure of the cardiac function in RV after SARS-CoV-2 infection. The highly expressed proteins of LA microvessels were the least expressed among the four heart regions (Figures 5B and S5B). However, the inflammatory response, innate immunity, and virus process-associated proteins in LA were upregulated mostly in COVID-19 hearts (Figure 7B), possibly because of the microvessels in LA being connected to the pulmonary vein, which is more vulnerable to the virus infecting the lung and its inflammatory storm. After oxygenated blood from the LA reached the LV, the microvessels of the LV contained many upregulated proteins that are associated with inflammation. Subsequently, the cell adhesion function, which is related to injury repair, as well as enzyme activity-associated proteins, which are related to vascular regeneration, were seriously disabled, indicating that the wound healing ability of microvessels in LV decreased after SARS-CoV-2 infection. Multiple molecular features explained the pathogenesis and the major clinical manifestations driven by SARS-CoV-2, providing a potential direction for the research and clinical treatment of heart diseases in the future.

Limitations of the study

Limitations of the current study include the limited coverage and depth of protein identification because of the paraffin section samples, especially the microvascular samples, obtained by microdissection. Nonetheless, the region-specific proteome datasets of COVID-19 myocardia and microvessels reported here provide a starting point for ascertaining the pathological characteristics of specific anatomical structures in hearts of patients with COVID-19. In addition, in this study, we observed the protein particles of SARS-CoV-2 and inflammatory cells in the microvessels of COVID-19 hearts. There remains a need to explore the specific mechanisms of injuries in COVID-19 hearts, such as the differences between the pathogenic mechanism of direct virus infection and inflammation, which can provide accurate intervention strategies for subsequent treatment.

STAR★METHODS

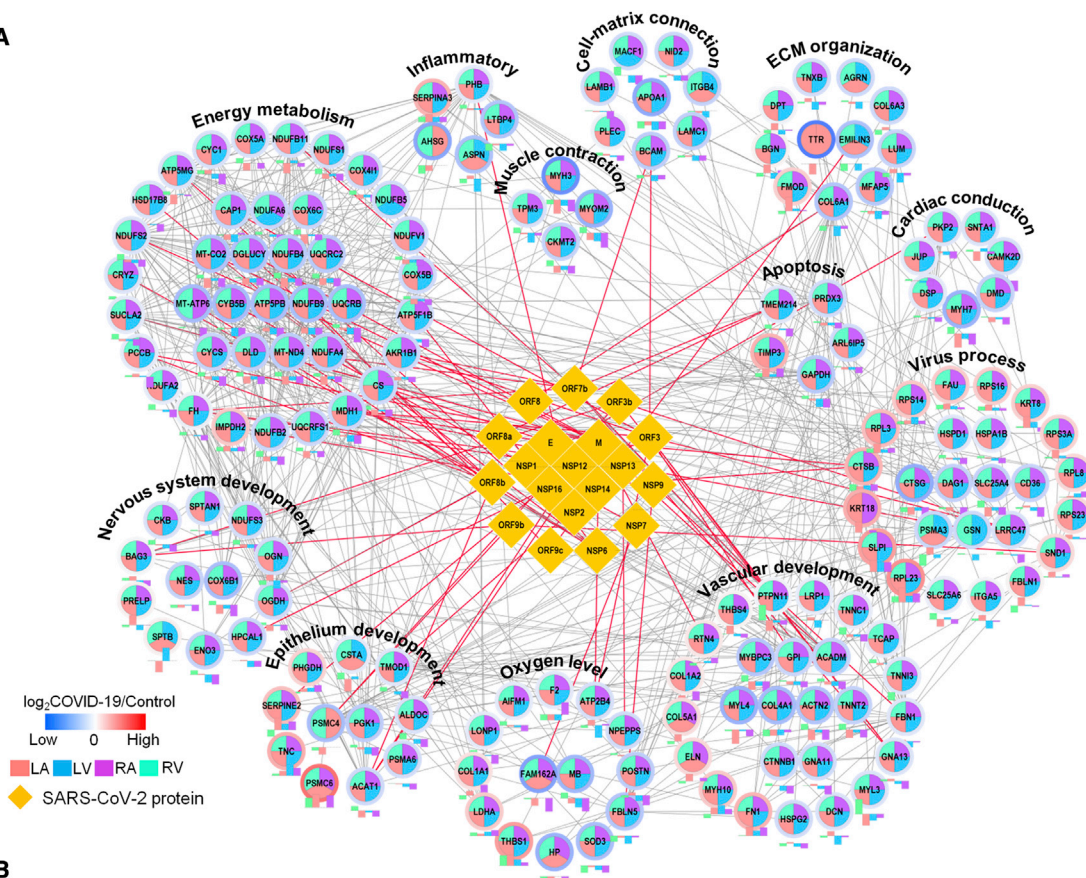
Detailed methods are provided in the online version of this paper and include the following:

with the moderated t test $p < 0.05$. The dysregulated proteins in the 10 clusters are labeled as circles (solid, upregulated proteins; hollow, downregulated proteins). The size of the circle indicates $|\log_2(\text{COVID-19/control})|$. The function items of the 10 clusters are presented at the top left corner. The red and blue boxes represent the upregulated and downregulated proteins, respectively, in the COVID-19 MVs, compared with the normal controls based on the protein numbers. (B) Function analysis of DEPs between COVID-19 MVs and control samples. Columns on the right of the heatmap represent different functional categories. The left of the heatmap presents the gene names. Red and blue boxes indicate the $\log_2(\text{COVID-19/control})$ of the upregulated or downregulated proteins, respectively. Asterisks indicate statistical significance ($*p < 0.05$; $**p < 0.01$; $***p < 0.001$), which were determined by the BH-adjusted p value of a moderated t test between COVID-19 and control samples.

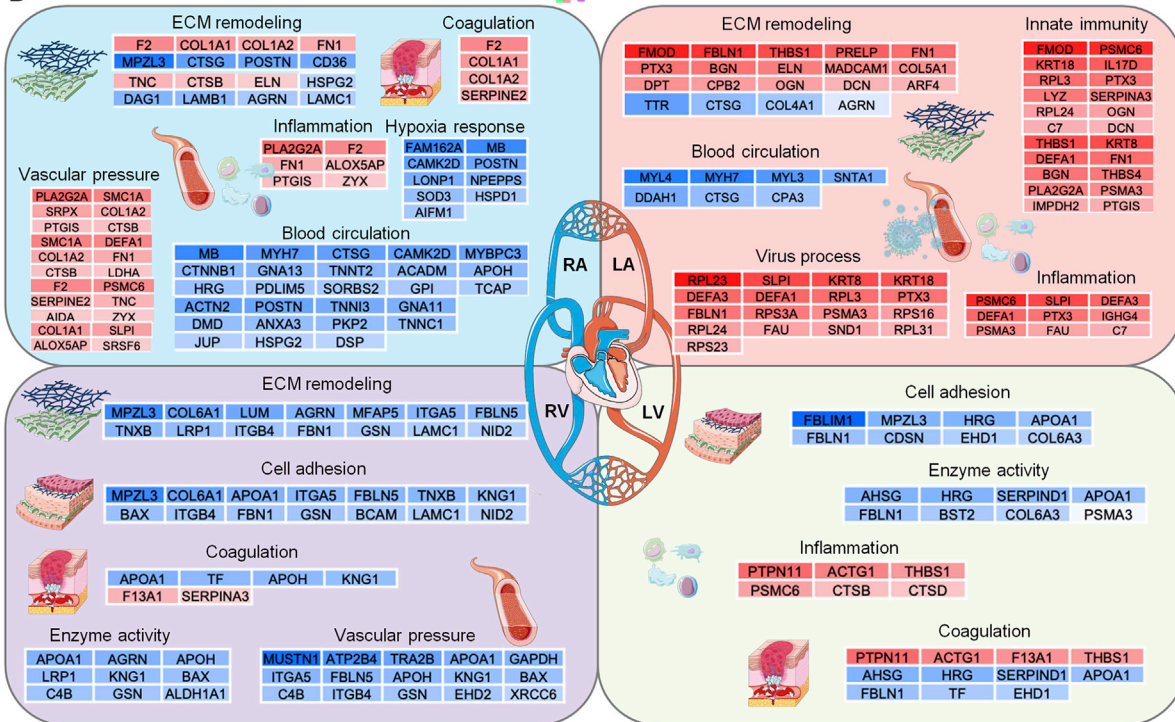
(C) Circos diagram shows upregulated and downregulated proteins that are involved in multiple biological processes of MVs from four heart regions in patients with COVID-19, compared with the normal controls. Red, green, blue, and purple lines represent the correlations between multiple biological processes and LA, LV, RA, and RV regions, respectively. Upregulated expressed proteins: moderated t test $p < 0.05$ and $\log_2(\text{COVID-19/control}) > 1$; downregulated expressed proteins: moderated t test $p < 0.05$ and $\log_2(\text{COVID-19/control}) < -1$.

See also Figures S4–S7.

A



B



(legend on next page)

- KEY RESOURCES TABLE
- RESOURCE AVAILABILITY
 - Lead contact
 - Materials availability
 - Data and code availability
- EXPERIMENTAL MODEL AND SUBJECT DETAILS
 - Human participants
- METHOD DETAILS
 - Laser-capture microdissection of heart samples
 - Histology and immunohistochemistry
 - Sample preparation for mass spectrometry analysis
 - Mass spectrometry acquisition
 - Mass spectrometry data analysis
- QUANTIFICATION AND STATISTICAL ANALYSIS

SUPPLEMENTAL INFORMATION

Supplemental information can be found online at <https://doi.org/10.1016/j.celrep.2022.110955>.

ACKNOWLEDGMENTS

This work was supported by Chinese Academy of Medical Sciences (CAMS) Endowment Fund (2021-CAMS-JZ004), CAMS Innovation Fund for Medical Sciences (2020-I2M-CoV19-001), Emergency Key Program of Guangzhou Laboratory (EKP21-32), the COVID-19 project from the Army Medical University (2020XGBD08), and National Science and Technology Major Project (2021YFA1301603).

AUTHOR CONTRIBUTIONS

L.L., S.-Y.Z., X.-W.B., and Z.-Y.L. conceived the overall study and designed experiments. L.L., J.M., X.L., M.-S.L., and Y.-P.Z. performed proteomics experiments and bioinformatics analysis. X.-W.B., P.-P.Z., J.C., R.T., L.Z., Z.-C.H., T.-R.L., H.-B.W., Y.-F.P., X.-H.Y., C.-H.Z., H.-T.G., and L.-Y.T. participated in COVID-19 tissues preparation. P.-P.Z. performed the laser-capture microdissection of COVID-19 heart samples. Z.-Y.L., Y.J., H.Z., and L.-R.Z. participated in non-COVID-19 controls tissues preparation. S.-C.X. performed the laser-capture microdissection of non-COVID-19 heart samples. P.-P.Z., L.L., Z.-H.W., and Y.-J.W. performed most of pathological staining experiments. L.L., J.M., X.L., and X.-W.B. wrote and edited the manuscript. S.-Y.Z., X.-W.B., and Z.-Y.L. conceived and supervised the data analysis. All authors made important comments to the manuscript.

DECLARATION OF INTERESTS

The authors declare no competing interests.

Received: February 16, 2022

Revised: April 28, 2022

Accepted: May 23, 2022

Published: May 27, 2022

REFERENCES

- Akhmerov, A., and Marbán, E. (2020). COVID-19 and the heart. *Circ. Res.* *126*, 1443–1455. <https://doi.org/10.1161/circresaha.120.317055>.
- Amengual, J., Guo, L., Strong, A., Madrigal-Matute, J., Wang, H., Kaushik, S., Brodsky, J.L., Rader, D.J., Cuervo, A.M., and Fisher, E.A. (2018). Autophagy is required for sortilin-mediated degradation of apolipoprotein B100. *Circ. Res.* *122*, 568–582. <https://doi.org/10.1161/circresaha.117.311240>.
- Angeli, F., Spanevello, A., De Ponti, R., Visca, D., Marazzato, J., Palmiotto, G., Feci, D., Reboldi, G., Fabbri, L.M., and Verdecchia, P. (2020). Electrocardiographic features of patients with COVID-19 pneumonia. *Eur. J. Intern. Med.* *78*, 101–106. <https://doi.org/10.1016/j.ejim.2020.06.015>.
- Barfield, D.Y., Puckelwartz, M.J., Kim, E.Y., Wilsbacher, L.D., Vo, A.H., Waters, E.A., Earley, J.U., Hadhazy, M., Dellefave-Castillo, L., Pesce, L.L., and McNally, E.M. (2017). Experimental modeling supports a role for MyBP-HL as a novel myofibrillar component in arrhythmia and dilated cardiomyopathy. *Circulation* *136*, 1477–1491. <https://doi.org/10.1161/circulationaha.117.028585>.
- Berk, B.C., Fujiwara, K., and Lehoux, S. (2007). ECM remodeling in hypertensive heart disease. *J. Clin. Invest.* *117*, 568–575. <https://doi.org/10.1172/jci31044>.
- Bojkova, D., Klann, K., Koch, B., Wiedera, M., Krause, D., Ciesek, S., Cinatl, J., and Münch, C. (2020). Proteomics of SARS-CoV-2-infected host cells reveals therapy targets. *Nature* *583*, 469–472. <https://doi.org/10.1038/s41586-020-2332-7>.
- Bonow, R.O., Fonarow, G.C., O’Gara, P.T., and Yancy, C.W. (2020). Association of coronavirus disease 2019 (COVID-19) with myocardial injury and mortality. *JAMA Cardiol.* *5*, 751–753. <https://doi.org/10.1001/jamacardio.2020.1105>.
- Bozaoglu, K., Curran, J.E., Stocker, C.J., Zaibi, M.S., Segal, D., Konstantopoulos, N., Morrison, S., Carless, M., Dyer, T.D., Cole, S.A., et al. (2010). Chemerin, a novel adipokine in the regulation of angiogenesis. *J. Clin. Endocrinol. Metab.* *151*, 2397–2485. <https://doi.org/10.1210/endo.151.5.9994>.
- Chung, M.K., Zidar, D.A., Bristow, M.R., Cameron, S.J., Chan, T., Harding, C.V., 3rd, Kwon, D.H., Singh, T., Tilton, J.C., Tsai, E.J., et al. (2021). COVID-19 and cardiovascular disease: from bench to bedside. *Circ. Res.* *128*, 1214–1236. <https://doi.org/10.1161/CIRCRESAHA.121.317997>.
- Driggin, E., Madhavan, M.V., Bikdeli, B., Chuich, T., Laracy, J., Biondi-Zoccai, G., Brown, T.S., Der Nigoghossian, C., Zidar, D.A., Haythe, J., et al. (2020). Cardiovascular considerations for patients, health care workers, and health systems during the COVID-19 pandemic. *J. Am. Coll. Cardiol.* *75*, 2352–2371. <https://doi.org/10.1016/j.jacc.2020.03.031>.
- Fan, D., Takawale, A., Lee, J., and Kassiri, Z. (2012). Cardiac fibroblasts, fibrosis and extracellular matrix remodeling in heart disease. *Fibrogenesis Tissue Repair* *5*, 15. <https://doi.org/10.1186/1755-1536-5-15>.
- Friedrich, M.G., and Cooper, L.T. (2021). What we (don’t) know about myocardial injury after COVID-19. *Eur. Heart J.* *42*, 1879–1882. <https://doi.org/10.1093/eurheartj/ehab145>.
- Gu, Z., Gu, L., Eils, R., Schlesner, M., and Brors, B. (2014). Circlize Implements and enhances circular visualization in R. *Bioinformatics* *30*, 2811–2812. <https://doi.org/10.1093/bioinformatics/btu393>.
- Guo, T., Fan, Y., Chen, M., Wu, X., Zhang, L., He, T., Wang, H., Wan, J., Wang, X., and Lu, Z. (2020). Cardiovascular implications of fatal outcomes of patients

Figure 7. Interaction network revealing dysregulated proteins in patients with COVID-19 MVs

(A) Interaction network of proteins that are differentially expressed in the MVs of four heart regions from patients diagnosed with COVID-19 versus control groups and SARS-CoV-2 proteins. A map of the functional categories was used for primary biological process analyses. Different regions are labeled with different colors. Red and blue rings of each circle represent proteins with high and low expressions, respectively, in the COVID-19 MVs compared with those of the normal controls; color depth indicates the high and low level of the protein abundance ratio (\log_2 COVID-19/control). The yellow diamond represents the structural, non-structural, and additional open reading frame proteins of SARS-CoV-2. Gray solid lines represent interactions between the virus proteins and reported virus-interacting proteins.

(B) Overview of biological processes based on proteome analysis of COVID-19 MVs. Alterations are defined by upregulated or downregulated proteins with red and blue boxes, respectively, according to \log_2 COVID-19/control.

- with coronavirus disease 2019 (COVID-19). *JAMA Cardiol.* 5, 811–818. <https://doi.org/10.1001/jamacardio.2020.1017>.
- Gupta, A., Madhavan, M.V., Sehgal, K., Nair, N., Mahajan, S., Sehrawat, T.S., Bikdeli, B., Ahluwalia, N., Ausiello, J.C., Wan, E.Y., et al. (2020). Extrapulmonary manifestations of COVID-19. *Nat. Med.* 26, 1017–1032. <https://doi.org/10.1038/s41591-020-0968-3>.
- Hou, T., Jian, C., Xu, J., Huang, A.Y., Xi, J., Hu, K., Wei, L., Cheng, H., and Wang, X. (2016). Identification of EFHD1 as a novel Ca(2+) sensor for mitochondrial activation. *Cell Calcium* 59, 262–270. <https://doi.org/10.1016/j.ceca.2016.03.002>.
- Lee, C.Y., Huang, C.H., Rastegari, E., Rengganaten, V., Liu, P.C., Tsai, P.H., Chin, Y.F., Wu, J.R., Chiou, S.H., Teng, Y.C., et al. (2021). Tumor necrosis factor- α exacerbates viral entry in SARS-CoV2-infected iPSC-derived cardiomyocytes. *Int. J. Mol. Sci.* 22, 9869. <https://doi.org/10.3390/ijms22189869>.
- Leng, L., Cao, R., Ma, J., Lv, L., Li, W., Zhu, Y., Wu, Z., Wang, M., Zhou, Y., and Zhong, W. (2021). Pathological features of COVID-19-associated liver injury—a preliminary proteomics report based on clinical samples. *Signal Transduct. Target. Ther.* 6, 9. <https://doi.org/10.1038/s41392-020-00406-1>.
- Leng, L., Cao, R., Ma, J., Mou, D., Zhu, Y., Li, W., Lv, L., Gao, D., Zhang, S., Gong, F., et al. (2020). Pathological features of COVID-19-associated lung injury: a preliminary proteomics report based on clinical samples. *Signal Transduct. Target. Ther.* 5, 240. <https://doi.org/10.1038/s41392-020-00355-9>.
- Madjid, M., Safavi-Naeini, P., Solomon, S.D., and Vardeny, O. (2020). Potential effects of coronaviruses on the cardiovascular system: a review. *JAMA Cardiol.* 5, 831–840. <https://doi.org/10.1001/jamacardio.2020.1286>.
- Nie, X., Qian, L., Sun, R., Huang, B., Dong, X., Xiao, Q., Zhang, Q., Lu, T., Yue, L., Chen, S., et al. (2021). Multi-organ proteomic landscape of COVID-19 autopsies. *Cellule* 184, 775–791.e14. <https://doi.org/10.1016/j.cell.2021.01.004>.
- Ning, Q., Wu, D., Wang, X., Xi, D., Chen, T., Chen, G., Wang, H., Lu, H., Wang, M., Zhu, L., et al. (2022). The mechanism underlying extrapulmonary complications of the coronavirus disease 2019 and its therapeutic implication. *Signal Transduct. Target. Ther.* 7, 57. <https://doi.org/10.1038/s41392-022-00907-1>.
- Offermanns, S., Mancino, V., Revel, J.P., and Simon, M.J. (1997). Vascular system defects and impaired cell chemokinesis as a result of G α_{13} deficiency. *Science* 275, 533–536. <https://doi.org/10.1126/science.275.5299.533>.
- Ren, X., Wen, W., Fan, X., Hou, W., Su, B., Cai, P., Li, J., Liu, Y., Tang, F., Zhang, F., et al. (2021). COVID-19 immune features revealed by a large-scale single-cell transcriptome atlas. *Cell* 184, 5838. <https://doi.org/10.1016/j.cell.2021.10.023>.
- Reyes, A., Melchionda, L., Burlina, A., Robinson, A.J., Ghezzi, D., and Zeviani, M. (2018). Mutations in TIMM50 compromise cell survival in OxPhos-dependent metabolic conditions. *EMBO Mol. Med.* 10, e8698. <https://doi.org/10.15252/emmm.201708698>.
- Sandoval, Y., Januzzi, J.L., Jr., and Jaffe, A.S. (2020). Cardiac troponin for assessment of myocardial injury in COVID-19. *J. Am. Coll. Cardiol.* 76, 1244–1258. <https://doi.org/10.1016/j.jacc.2020.06.068>.
- Shannon, P., Markiel, A., Ozier, O., Baliga, N.S., Wang, J.T., Ramage, D., Amin, N., Schwikowski, B., and Ideker, T. (2003). Cytoscape: a software environment for integrated models of biomolecular interaction networks. *Genome Res.* 13, 2498–2504. <https://doi.org/10.1101/gr.1239303>.
- Shao, X., Taha, I.N., Clauser, K.R., Gao, Y.T., and Naba, A. (2020). MatrismoDB: the ECM-protein knowledge database. *Nucleic Acids Res.* 48, D1136–D1144. <https://doi.org/10.1093/nar/gkz849>.
- Sharma, A., Garcia, G., Jr., Wang, Y., Plummer, J.T., Morizono, K., Arumugawami, V., and Svendsen, C.N. (2020). Human iPSC-derived cardiomyocytes are susceptible to SARS-CoV-2 infection. *Cell Rep. Med.* 1, 100052. <https://doi.org/10.1016/j.xcrm.2020.100052>.
- Sherman, B.T., Hao, M., Qiu, J., Jiao, X., Baseler, M.W., Lane, H.C., Imamichi, T., and Chang, W. (2022). DAVID: a web server for functional enrichment analysis and functional annotation of gene lists (2021 update). *Nucleic Acids Res.* 23, gkac194. <https://doi.org/10.1093/nar/gkac194>.
- Shu, T., Ning, W., Wu, D., Xu, J., Han, Q., Huang, M., Zou, X., Yang, Q., Yuan, Y., Bie, Y., et al. (2020). Plasma proteomics identify biomarkers and pathogenesis of COVID-19. *Immunity* 53, 1108–1122.e5. <https://doi.org/10.1016/j.immuni.2020.10.008>.
- Stukalov, A., Girault, V., Grass, V., Karayel, O., Bergant, V., Urban, C., Haas, D.A., Huang, Y., Oubraham, L., Wang, A., et al. (2021). Multilevel proteomics reveals host perturbations by SARS-CoV-2 and SARS-CoV. *Nature* 594, 246–252. <https://doi.org/10.1038/s41586-021-03493-4>.
- Sungnak, W., Huang, N., Bécavin, C., Berg, M., Queen, R., Litvinukova, M., Talavera-López, C., Maatz, H., Reichart, D., Sampaziotis, F., et al. (2020). SARS-CoV-2 entry factors are highly expressed in nasal epithelial cells together with innate immune genes. *Nat. Med.* 26, 681–687. <https://doi.org/10.1038/s41591-020-0868-6>.
- Szklarczyk, D., Morris, J.H., Cook, H., Kuhn, M., Wyder, S., Simonovic, M., Santos, A., Doncheva, N.T., Roth, A., Bork, P., et al. (2017). The STRING database in 2017: quality-controlled protein-protein association networks, made broadly accessible. *Nucleic Acids Res.* 45, D362–D368. <https://doi.org/10.1093/nar/gkw937>.
- Tretter, J.T., and Redington, A.N. (2018). The forgotten ventricle? the left ventricle in right-sided congenital heart disease. *Circ. Cardiovasc. Imaging* 11, e007410. <https://doi.org/10.1161/circimaging.117.007410>.
- Ulisse, V., Dey, S., Rothbard, D.E., Zeevi, E., Gokhman, I., Dadosh, T., Minis, A., and Yaron, A. (2020). Regulation of axonal morphogenesis by the mitochondrial protein Efh1. *Life Sci. Alliance* 3, e202000753. <https://doi.org/10.26508/lsa.202000753>.
- Yao, X.H., Luo, T., Shi, Y., He, Z.C., Tang, R., Zhang, P.P., Cai, J., Zhou, X.D., Jiang, D.P., Fei, X.C., et al. (2021). A cohort autopsy study defines COVID-19 systemic pathogenesis. *Cell Res.* 31, 836–846. <https://doi.org/10.1038/s41422-021-00523-8>.
- Zhang, F., Ge, W., Ruan, G., Cai, X., and Guo, T. (2020). Data-independent acquisition mass spectrometry-based proteomics and software tools: a Glimpse in 2020. *Proteomics* 20, e1900276. <https://doi.org/10.1002/pmic.201900276>.

STAR★METHODS

KEY RESOURCES TABLE

REAGENT or RESOURCE	SOURCE	IDENTIFIER
Antibodies		
TFRC	PROTEINTECH	Cat# 10084-2-AP; RRID: AB_2240403
SF3B2	PROTEINTECH	Cat# 10919-1-AP; RRID: AB_2285782
Spike	Sino Biological	Cat# 40150-T62-COV2
PRKCSH	PROTEINTECH	Cat# 12148-1-AP; RRID: AB_2253107
PGD	PROTEINTECH	Cat# 14718-1-AP; RRID: AB_2236801
Biological samples		
Autopsy cases of deceased patients with COVID-19	Third Military Medical University (Army Medical University)	This paper (Table S1)
Puncture samples as non-COVID-19 controls	Peking Union Medical College Hospital	This paper (Table S2)
Chemicals, peptides, and recombinant proteins		
Hematoxylin-Eosin (HE) Stain Kit	MKBio	MM1031-1L
Eostin	Solarbio	G1100
Deposited data		
Mass spectrometry data	https://www.iprox.cn	PXD031249/IPX0004043000
Mendeley Data	https://data.mendeley.com/	http://dx.doi.org/10.17632/4r7mtm9gdh.1
Software and algorithms		
Cytoscape	Cytoscape Consortium	version 3.8.2
DAVID	Laboratory of Human Retrovirology and Immunoinformatics	https://david.ncifcrf.gov/
MatrisomeDB	Matrisome Project	http://matrisomeproject.mit.edu/
R package Limma	R Project	version 3.50.0
R package ape	R Project	version 5.4.1
R package ComplexHeatmap	R Project	version 2.10.0
R package circlize	R Project	version 0.4.13
STRING database	STRING Consortium	https://string-db.org/
UniProt	UniProt Consortium	https://www.uniprot.org/

RESOURCE AVAILABILITY

Lead contact

Further information and requests for resources and reagents should be directed to and will be fulfilled by the lead contact Shuyang Zhang (shuyangzhang103@nrdrs.org).

Materials availability

This study did not generate new unique reagents.

Data and code availability

All proteomics raw data have been deposited to the ProteomeXchange Consortium via the iProX partner repository with the dataset identifier PXD031249/IPX0004043000. Additional Supplemental Items are available from Mendeley Data at <http://dx.doi.org/10.17632/4r7mtm9gdh.1>.

This paper does not report original code.

Any additional information required to reanalyze the data reported in this paper is available from the [lead contact](#) upon request.

EXPERIMENTAL MODEL AND SUBJECT DETAILS

Human participants

Hearts were obtained from five autopsy cases of deceased patients with COVID-19, including one male and four females with the age ranging from 57 to 80 (clinical data is shown in [Table S1](#)). Autopsies were performed 8–24 h after death in Wuhan, China, from February 18 to April 4, 2020. The puncture samples of heart tissues from 30 individuals were collected as non-COVID-19 controls at the Department of Pathology, Peking Union Medical College Hospital, including 12 males and 18 females with the age ranging from 19 to 75 (clinical data is shown in [Table S2](#)). All samples and clinical data were obtained with informed consents provided by their guardians and the procedures were performed in accordance with cohort hospital ethics committee regulations and the National Health Commission of China and the Helsinki Declaration. Samples from the four heart regions, including the LA, LV, RA, and RV, were used for histopathological examination and proteomics analysis.

METHOD DETAILS

Laser-capture microdissection of heart samples

In histopathology, the myocardia and microvessels are totally different and can be distinguished completely. Thus, the pathologists participated in this study were requested to separate the myocardium and microvessels accurately according to the histopathology and then performed the laser-capture microdissection to different parts of myocardia and microvessels. Myocardia are the main components of the heart. We selected myocardial tissues without microvessels as myocardial samples. The microvessels in the myocardia were cut along with the adventitia to avoid mixing with the surrounding tissues ([Video S1](#)). For each sample, we collected multiple parts of microvessels to ensure the integrity of the overall vascular tissues. According to the pathology analysis, the 10 μm section was used for laser microdissection and collection of microvessels. All parts of myocardial or microvessels of two sections were collected for MS analysis.

The laser-capture microdissection of heart samples from different regions were obtained according to the following procedure ([Video S1](#)). The FFPE heart samples were cut and mounted on an Molecular Machines and Industries (MMI) MembraneSlides (MMI GmbH, Eching, Germany) after hematoxylin-eosin (H&E) staining. Laser-capture microdissection was performed using a laser microdissection system from MMI CellCut Laser Microdissection, Eching, Germany controlled by the MMI Cell Tools software from the same company. After calibrating the laser focus and power, we cut the left atrial myocardium (LA_MC), left atrial microvessel (LA_MV), left ventricular myocardium (LV_MC), left ventricular microvessel (LV_MV), right atrial myocardium (RA_MC), right atrial microvessel (RA_MV), right ventricular myocardium (RV_MC), and right ventricular microvessel (RV_MV).

Histology and immunohistochemistry

The heart samples were processed as formalin-fixed, paraffin-embedded tissue blocks. H&E and immunohistochemical stains on 4- μm slides were performed according to the standard procedure, as previously described ([Ren et al., 2021](#); [Yao et al., 2021](#)). The primary antibodies included TFRC, SF3B2, PRKCSH, and PDG. The immunostaining results were semi-quantitatively evaluated as partially positive (<50% of stained cells) or diffusely positive (\geq 50% of stained cells).

Sample preparation for mass spectrometry analysis

The H&E-stained tissue sections were first destained with a 99:1 mixture of 70% ethanol and hydrochloric acid. After that, tissue samples were performed in treatment solution (50% [v/v] mixture of 50 mM ammonium bicarbonate and trifluoroethanol [TFE]) for 45 min at 90°C. The tissue lysate was reduced at 25 mM dithiothreitol (1 h at 37°C) and afterward alkylated at 50 mM iodoacetamide (30 min in darkness at room temperature). Upon vacuum centrifugation, digestion was conducted in 5% TFE, 50 mM ABC, trypsin was added at a ratio of 1:50 (enzyme to protein) at 37°C for 14–16 h. Digestions were stopped by adding trifluoroacetic acid to obtain a final concentration of 0.5%. The peptides were desalted using Ziptip C18 pipette tips (Millipore, USA) according to the manufacturer's instructions. After drying, the peptides were resuspended in 0.1% formic acid. Then, 1 μg of protein lysate from each sample were removed for DIA Spectral Library building. The Biognosys iRT Kit was added to remaining samples according to the manufacturer's instructions (required for DIA analysis using Biognosys Spectronaut).

Mass spectrometry acquisition

The samples were analyzed using a homemade analytical column (150 μm \times 170 mm, 1.9 μm) on an EASY-nLC1200 connected to an Orbitrap Exploris 480 mass spectrometer (Thermo Scientific). Peptides were eluted using a binary solvent system with 99.9% H₂O, 0.1% formic acid (phase A), 80% ACN, 19.9% H₂O, and 0.1% formic acid (phase B). The following linear gradient was used: 8%–28% B for 44 min, 28%–35% B for 7 min, 35%–100% B for 3 min, washed at 100% B for 9 min for microvessels and 11 min for myocardia. The eluent was introduced directly to an Orbitrap Exploris480 mass spectrometer via an EASY-Spray ion source. Source ionization parameters were as follows: spray voltage, 2.3 kV; capillary temperature, 350°C.

For the DDA-MS runs, MS spectra were collected in the Orbitrap mass analyzer (60,000 resolutions, 300–1350 m/z range) with an AGC target of 3×10^6 and a maximum ion injection time of 22 ms. For HCD, the isolation window was set to 1.6 m/z and normalized collision energy of 28% was applied. MS/MS spectra were collected in the Orbitrap (15,000 resolution) with an AGC target of 7.5×10^4 and a maximum ion injection time of 22 ms.

The DIA-MS method consisted of an MS1 scan from 300 to 1300 m/z (AGC target 3×10^6 and 28 ms injection time). Then, DIA segments were acquired at a resolution of 15,000 (AGC target 1×10^6 and maximum injection time mode was set to auto). The collision energy was 32%. The spectra were recorded in profile mode. The default charge state for the MS2 was set to 3.

Mass spectrometry data analysis

DIA data were analyzed with a Spectronaut pulsar, a mass spectrometer vendor independent software from Biognosys (Zhang et al., 2020). The default settings were used for targeted analysis of DIA data in Spectronaut. In brief, the retention time prediction type was set to dynamic iRT (adapted variable iRT extraction width for varying iRT precision during the gradient) with a correction factor applied to the window. Mass calibration was set to local mass calibration. Decoy generation was set to scrambled (no decoy limit). Interference correction on the MS2 level was enabled, removing fragments from quantification based on the presence of interfering signals but keeping at least three fragments for quantification. The false discovery rate was estimated using the prophet approach and set to 1% at the peptide level. Protein inference to determine the protein groups was performed using the principle of parsimony with the ID picker algorithm as implemented in Spectronaut. For the analysis of the DIA-runs with the spectral library, the RAW files were converted into the Spectronaut file format, and then the files were calibrated in the retention time dimension using the global spectral library. Subsequently, the recalibrated files were used for targeted data analysis with the spectral library without new recalibration of the retention time dimension. The DDA files were searched against the UniProt human database (downloaded on 11th Dec. 2020) and the Biognosys iRT peptides sequences database.

QUANTIFICATION AND STATISTICAL ANALYSIS

The quantification values of the identified proteins were normalized by taking the fraction of the total, which was multiplied by 10^6 and log2 transformed. Pairwise comparisons to determine the proteins whose expression was significantly different between the COVID-19 patients and normal controls were performed by a moderated *t* test using the R package Limma (version 3.50.0) in Figures 1C and 1D, 4, 6, S1G, S3E, S4, S5E, and S7. One-way ANOVA was used to determine whether there are any statistically significant differences in the normalized intensities among four heart regions of myocardia (Figure 3A) and microvessels (Figure 5A). Differences according to the Benjamin–Hochberg adjusted *p* value of <0.05 (*), 0.01 (**), or 0.001 (***) were considered statistically significant, and the specific *p* value is indicated in the figure legends separately.

The online tool DAVID (<https://david.ncifcrf.gov/>) (Sherman et al., 2022) was used to annotate the proteins according to biological processes and cellular components via GO analysis. PCoA of the proteins whose values in each sample were valid was performed using the R package ape (version 5.4.1). The protein–protein interactions were retrieved from the STRING database (<https://string-db.org/>) (Szklarczyk et al., 2017) and the network was built using Cystoscope (version 3.8.2) (Shannon et al., 2003). We used the ComplexHeatmap package (version 2.10.0) to reveal the specificity proteins in region-resolved myocardia and microvessel. We also used the circlize package (Gu et al., 2014) (version 0.4.13) to circularly visualize upregulated and downregulated proteins that are involved in multiple biological processes associated with four heart regions.